Catalysis Today 170 (2011) 33–39

Contents lists available at ScienceDirect

Catalysis Today

journal homepage: www.elsevier.com/locate/cattod

Ni–Co–B catalyst-promoted hydrogen generation by hydrolyzing $NaBH_4$ solution for in situ hydrogen supply of portable fuel cells

Chuan Wu[a,*], Ying Bai[a], Dan-Xian Liu[a], Feng Wu[a], Mei-Li Pang[a], Bao-Lian Yi[b]

[a] School of Chemical Engineering and the Environment, Beijing Institute of Technology, Beijing 100081, PR China
[b] Lab of PEMFC Key Material and Technologies, Dalian Institute of Chemical Physics, Chinese Academy of Sciences, Dalian 116023, PR China

ARTICLE INFO

Article history:
Received 30 October 2010
Received in revised form 22 January 2011
Accepted 24 January 2011
Available online 5 March 2011

Keywords:
Proton-exchange membrane fuel cell
Ni–Co–B catalyst
Surface
Hydrogen generation
$NaBH_4$
Hydrolysis

ABSTRACT

A series of Ni–Co–B catalysts were synthesized by a two-step technique, namely, chemical reduction was used to prepare the precursors, and heat-treatment was used to adjust the crystal structures. The structures of the as-prepared Ni–Co–B catalysts were characterized by X-ray diffraction (XRD), scanning electron microscopy (SEM), X-ray photoelectron spectroscopy (XPS), and nitrogen adsorption–desorption test. The catalytic activities of the Ni–Co–B catalysts for $NaBH_4$ hydrolysis were evaluated in a successive hydrogen generation mode, where a 5%$NaBH_4$ + 1%NaOH solution was pumped into the hydrogen generation reactor with a feeding rate of 5 ml per minute. It is found that the heat-treatment affects the crystal structure, the apparent morphology, the oxidation state, the surface structure, as well as the hydrogen generation performances of the Ni–Co–B catalysts. The sample treated at 673 K achieves an average hydrogen generation rate of 708 ml min^{-1} $g^{-1}_{catalyst}$, which can give successive hydrogen supply for an 115 W portable proton-exchange membrane fuel cell (PEMFC).

1. Introduction

Nowadays, the proton-exchange membrane fuel cell (PEMFC) is attracting widely attention as a zero-emission high efficient energy source. In situ hydrogen supply technique is one of the key issues for the commercialization of the PEMFC. Recently, hydrogen generation from $NaBH_4$ hydrolysis is proved to be a feasible hydrogen supply method for the PEMFC [1], which can be promoted by using ex situ [1–7] or in situ [8–11] synthesized catalysts during the hydrogen generation reaction. Also, the by-product $NaBO_2$ is environmentally clean and can be recycled for synthesizing $NaBH_4$ [12]. Therefore, $NaBH_4$ hydrolysis is regarded as an efficient and environmental friendly hydrogen generation method and catches more and more attention.

Catalytic strategy is one of the crucial issues for sustainable hydrogen supply from $NaBH_4$ hydrolysis. In recent years, metal borides were studied extensively as high efficient catalysts for $NaBH_4$ hydrolysis, among which cobalt boride-based catalysts are the most attractive ones [2,5,7,13–19]. To meet the requirements of practical applications, some other metal borides, such as nickel boride [20,21] and ferric boride [8], were also evaluated. In 2007, Ingersoll et al. [22] found that the catalyst Ni–Co–B that could positively contribute to an enhanced efficiency of hydrogen generation. More recently, Fernandes et al. [23] indicated that the presence of mixed Co–Ni with B atoms results in an enhanced catalytic effect with respect to Co–B or Ni–B powders. However, they plot the time dependences versus stoichiometric hydrogen production yield (%) instead of hydrogen volume (ml), which is visual and intuitionistic for evaluating the practical use potential of the catalysts. In this paper, in order to investigate the optimum heat-treating condition and evaluate the potential for portable fuel cell applications, we will discuss the effect of heat-treatment on the structure and catalytic performance of composite Ni–Co–B catalysts, which has not been reported previously. Also, we will evaluate the corresponding fuel cell power with the hydrogen supply from $NaBH_4$ hydrolysis, which is catalyzed by Ni–Co–B catalysts. Herein, several Ni–Co–B catalysts with various heat-treating temperatures are prepared, characterized and compared.

2. Experimental

2.1. Ni–Co–B catalyst preparation

The precursors of the Ni–Co–B catalysts were prepared by a chemical reduction, where a 5%$NaBH_4$ + 1%NaOH solution was used as the reducing agent, and $CoCl_2$ and $NiCl_2$ with the ratio of 1:1 were selected as the metal sources. The mole ratio of $NaBH_4$ and the total metal atoms was set as 5:1 to ensure a complete reduction

* Corresponding author at: School of Chemical Engineering and the Environment, Beijing Institute of Technology, 5# South Zhongguancun Street, Beijing 100081, PR China. Tel.: +86 10 68912657; fax: +86 10 68451429.
E-mail address: chuanwu@bit.edu.cn (C. Wu).

0920-5861/$ – see front matter © 2011 Elsevier B.V. All rights reserved.
doi:10.1016/j.cattod.2011.01.046

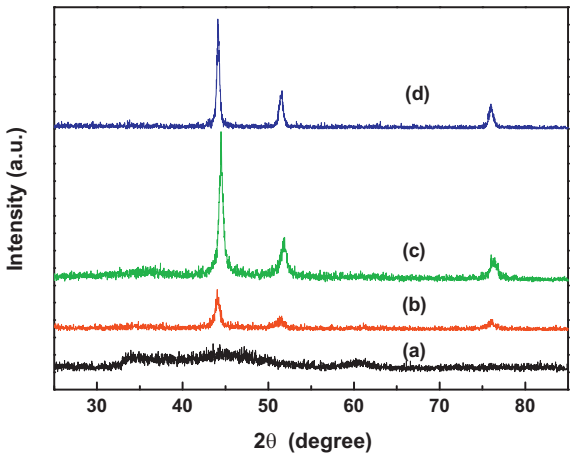

Fig. 1. XRD patterns of the Ni–Co–B catalysts heated at different temperatures: (a) 373 K; (b) 573 K; (c) 673 K; and (d) 773 K.

reaction. A 100 ml mixed solution of $CoCl_2$ and $NiCl_2$ was beforehand put into the reactor and stirred by a magnetic stirrer. A 100 ml 5%$NaBH_4$ + 1%NaOH solution was added into the reactor drop by drop with a peristaltic pump, and the time for reaction was 2 h. Dark precipitates were generated in this process. After the reaction, the precipitates were filtered, washed by deionized water, and vacuum-dried at 328 K for 12 h. The vacuum-dried precursors were put into a tube furnace and heated at various temperatures respectively under the protection of an argon atmosphere.

2.2. Structural characterization

Crystal structural characterization of the as-prepared Ni–Co–B catalyst was determined by a conventional X-ray diffraction using CuK_α radiation (XRD, Rigaku DMAX2400X). The scan range was set from 20° to 90°, and the scan rate was 8°/min in steps of 0.02°. The apparent morphology was observed on a scanning electronic microscope (SEM, Quanta 600). The surface electronic states were carried out by X-ray photoelectron spectroscopy (XPS, SCIENTAESCA200). The XPS spectra were acquired within an instrument equipped with a monochromatic Al K_α (1486.6 eV) X-ray source and a hemispherical analyzer. Nitrogen adsorption–desorption test was measured with a surface area and pore size analyzer (Nova 1200e). The specific surface areas of the catalysts were determined from the N_2 adsorption–desorption isotherms by the BET method.

2.3. Hydrogen generating test

To evaluate the catalytic activity, a sample of 100 mg Ni–Co–B catalyst was introduced to a dry hydrogen generating reactor, and a small amount of deionized water was added to make it wet. Then a mixed 5%$NaBH_4$–10%NaOH solution was added drop by drop into the reactor by a peristaltic pump at a feeding rate of 5 ml min^{-1}. The solution and the catalyst inside the reactor were stirred by an electro-magnetic stirrer. During this process, H_2 was released from the vent. The as-generated H_2 was input into a surge flask to wash out the residual alkali and water, and then passed through a flow meter, where the accumulated H_2 volume was recorded. After reaction for 20 min, the pump was switched off. All the hydrolysis reactions were performed at 293 K.

3. Results and discussion

3.1. XRD patterns

Fig. 1 shows the XRD patterns of the Ni–Co–B catalysts heated at different temperatures. It can be seen that one relatively broad dispersing peak appears near $2\theta \approx 45°$ for the Ni–Co–B catalyst heated at 373 K, indicating an amorphous structure. Furthermore, according to a previous study, Geng et al. [24] used high-resolution

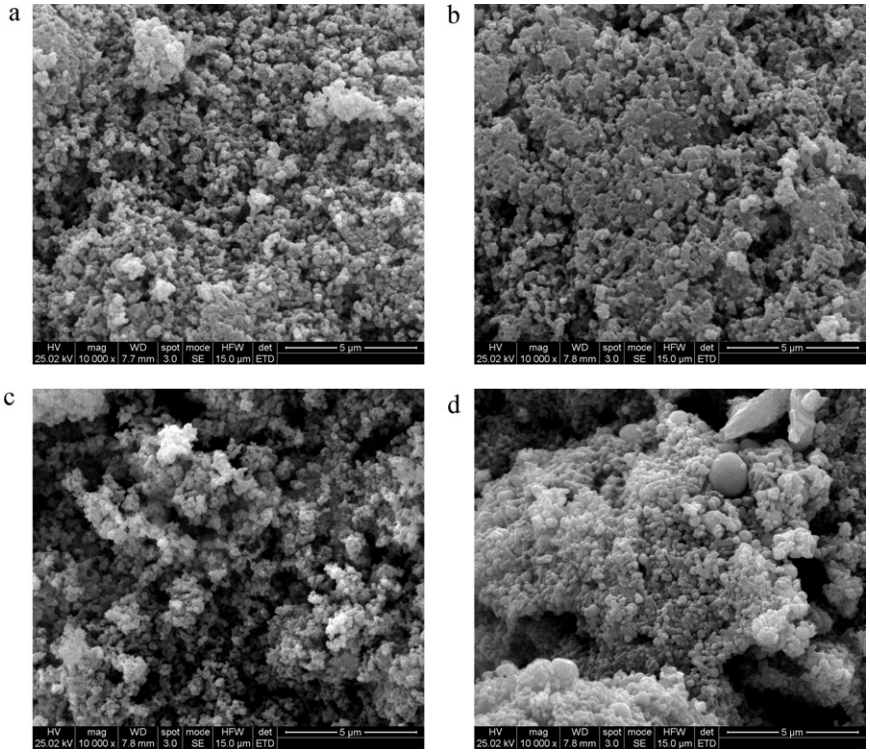

Fig. 2. SEM images of the Ni–Co–B catalysts heated at different temperatures: (a) 573 K; (b) 673 K; (c) 773 K; and (d) 973 K.

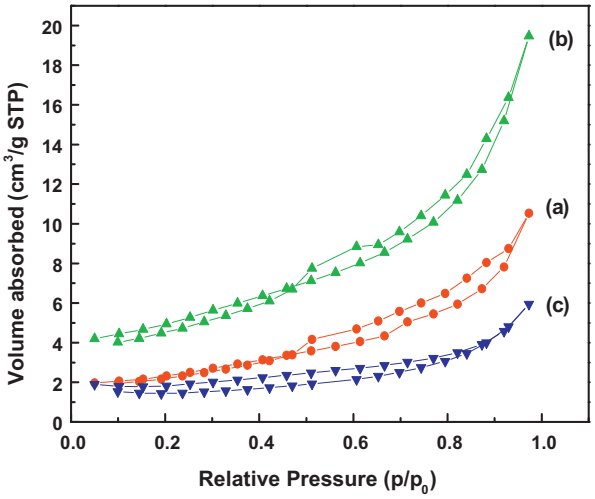

Fig. 3. Nitrogen adsorption–desorption curves of the Ni–Co–B catalysts heated at different temperatures: (a) 573 K; (b) 673 K; and (c) 773 K.

transmission electron microscopy (HRTEM) to observe the ultrafine crystalline structure of a Ni·B catalyst, and found that although the component nanoparticles are extremely small, they are nevertheless crystalline. Based on this point of view, here the Ni–Co–B catalysts may also have tiny Ni and Co crystallites bound in the matrix of boron-containing species. With increasing temperature, the dispersing peak disappears, and the diffractions of the Ni–Co–B compound gradually become sharpened, indicating the crystallization of the precursor, and the transformation from an amorphous phase to a crystal phase occurs. When the heating temperature gradually increases from 373 K to 573 K, the diffraction peaks emerge around $2\theta = 44.5$, 51.5 and 76.1 are very clear. According to the JCPDS database, the (1 1 1), (2 0 0), (2 2 0) diffractions of cubic Ni [25] are located at $2\theta = 44.496$, 51.849 and 76.381 respectively; while the (1 1 1), (2 0 0), (2 2 0) diffractions of cubic Co [26] are located at $2\theta = 44.216$, 51.522 and 75.853 respectively. The diffractions of metal Ni and Co are so closer, that they overlap with each other and cannot be distinctly identified in this case. At the same time, this phenomenon implies the formation of metal crystal states, especially a combination of metal Ni and Co, upon heat treating. The XRD patters of the Ni–Co–B catalysts here are very similar to those of crystal state Ni and Raney Ni [3], which confirm that the Ni–Co–B catalysts will decompose to metals at high temperatures. However, the hydrogen generation rates of the crystal state Ni and Raney Ni in previous study were only 19.5 and 228.5 ml min^{-1} $g^{-1}_{catalyst}$ respectively [3], while the hydrogen generation rates of the Ni–Co–B catalysts here are much higher, as described subsequently. Therefore, it indicates that these catalysts were obviously different from each other, indicating the existence of other crystal phases, such as Co, Co–B or Co–Ni–B [22], during the heat treatment of the Ni–Co–B catalyst. The formation of the cubic crystal systems of Co [26], Co–B [27,28] and Ni–B [29] as well as other crystal phases might also be found in the fine XRD patterns. But further studies should be carried out to confirm.

3.2. Apparent morphology

Fig. 2 shows the 10,000-fold SEM images of the Ni–Co–B catalysts treated at different temperatures. It is clear that Ni–Co–B treated at 573 K had relatively small and loosen alloy particles, taking on the characteristics of partial crystallization; when the temperature increases to 673 K, the Ni–Co–B particles cluster together to from agglomerations; when the temperature increases to 773 K, the particle agglomeration becomes obvious, indicating the characteristic of crystallization; when the temperature further increase to 973 K, the particle agglomeration is extremely serious in Ni–Co–B catalyst and large crystal pieces are precipitated.

3.3. Specific surface area

Since the activity of the catalyst is strongly related with the contact area between the catalyst and the reactant, the specific surface

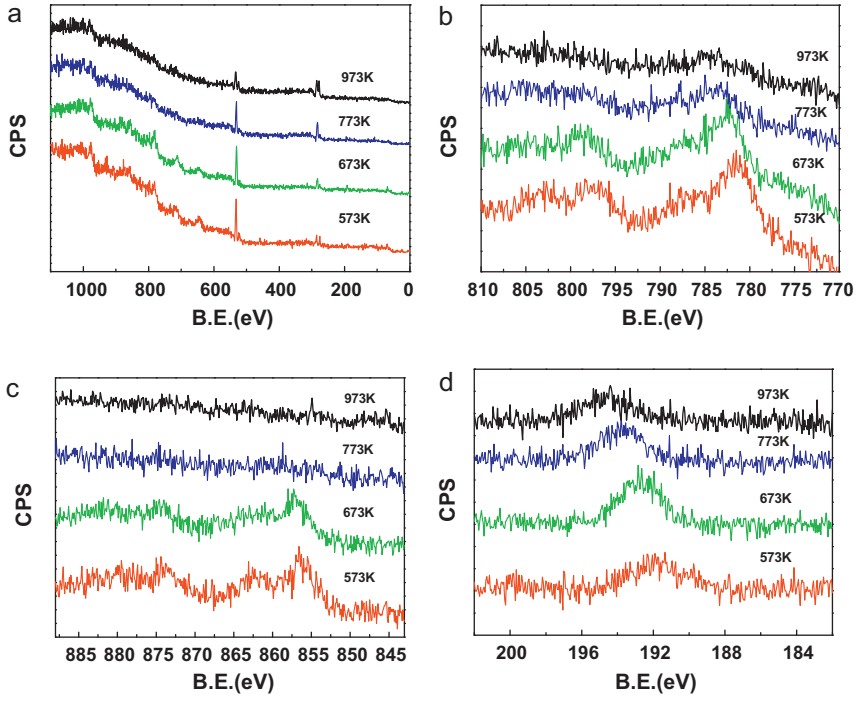

Fig. 4. X-ray photoelectron spectra of the Ni–Co–B catalysts heated at different temperatures: (a) Full XPS spectra; (b) Co(2p) emissionl; (c) Ni(2p) emission; and (d) B(1s) emission.

areas is a very important parameter for evaluating the catalyst. Here the BET surfaces of the Ni–Co–B catalysts were determined to further study the effect of different heating temperatures. The isothermal adsorption–desorption curves of the Ni–Co–B catalysts are shown in Fig. 3, These isothermals concave down during the whole pressure range, indicating they are of type III isothermal. Namely, the adsorption interaction between the sorbent nitrogen and the Ni–Co–B catalysts are weak. In addition, the adsorption capacities increase fleetly at high relative pressure range, illustrate the existence of the hole filling effect during adsorption. The Ni–Co–B catalyst treated at 673 K had the largest specific surface area, 17.07 $m^2\ g^{-1}$, indicating that when acting as the catalyst for hydrogen generation by hydrolyzing $NaBH_4$, it had the highest contact area with $NaBH_4$ solution, which may result in the best catalytic activity and the fastest chemical reaction. The specific surface areas of Ni–Co–B catalysts heat-treated at 573 K and 773 K are 8.20 and 5.94 $m^2\ g^{-1}$ respectively. It is mainly because the Ni–Co–B catalyst treated at elevated temperatures become crystallized, which result in bigger particle aggregations, and lead to the decreasing specific surface areas. This phenomenon is consistent with the XRD and SEM analysis. Furthermore, for the Ni–Co–B catalyst treated at 973 K, since it is so heavily crystallized, the specific area is out of the detection limit of the equipment, thus cannot be detected by nitrogen adsorption–desorption test, which is very similar to the Co–B alloy synthesized via the electric arc method [30].

3.4. XPS analysis

Fig. 4 shows the XPS emissions of the Ni–Co–B catalysts. Fig. 4(a)–(d) are the full spectra, the Co(2p) emission, the Ni(2p) emission, and the B(1s) emission, respectively. All the spectra are proofread by the binding energy of standard C(1s) reference at 284.6 eV. It is observed that the split of the emissions exist for both Co(2p) and Ni(2p) emissions, as shown in Fig. 4(b) and (c). The binding energies of the Ni(2p), Co(2p) and B(1s) emissions are all fitted from the XPS curves by Gaussian method. In order to better visualize the Gaussian fit, as well as avoid supplying too many reduplicate data, some examples of the Gaussian-fitted curves are shown in Fig. 5. The as-obtained binding energies are listed in Table 1. It can be seen that the Ni($2p_{3/2}$), Ni($2p_{1/2}$), Co($2p_{3/2}$), and Co($2p_{1/2}$) emissions are all split into two peaks, which indicate that there might be a co-existence of multiple valence species. When the heating temperature increase from 573 K to 673 K, the Ni($2p_{3/2}$) emission shift from 856.2 to 856.8 eV, while the Co($2p_{3/2}$) emission shift from 781.3 to 782.3 eV, and the B(1s) emission shift from 191.8 to 192.8 eV, namely, the XPS emissions of B(1s), Co(2p) and Ni(2p) are all have a positive tendency shift to higher binding energy, as shown in Figs. 4 and 5, which indicate the electrons of element B has transferred into the empty d orbits of Co and Ni, resulting in the lack of electrons in element B but enriched electrons in Co and Ni [23]. The existence of electrons can enrich the metal activity center repel oxygen atom, while strongly attracted element B lacking of electrons [31]. Therefore, the enhancement of M–B (M = Co, Ni) bonds is achieved, and multiplex metal borides with highly catalytic activities can be formed. In addition, for the B(1s) emission, the binding energy increases from 191.8 to 194.6 eV with increasing temperature, implies the boron species are also existed in oxidation states [32]. These data are very similar to the B–O bonds from 191.95 to 193.80 eV [33], and indicating there are abounding B–O bonds on the Ni–Co–B surface.

According to previous studies [34,35], hydrogen was the by-product for the synthesis of metal boride by $NaBH_4$ reduction method. That is to say, the synthesis process is carried on in a reductive atmosphere. The situation in this study is the same. Therefore, oxygen should not be introduced into the bulk phase of the Ni–Co–B precursors. Also, the heat-treating processing of the

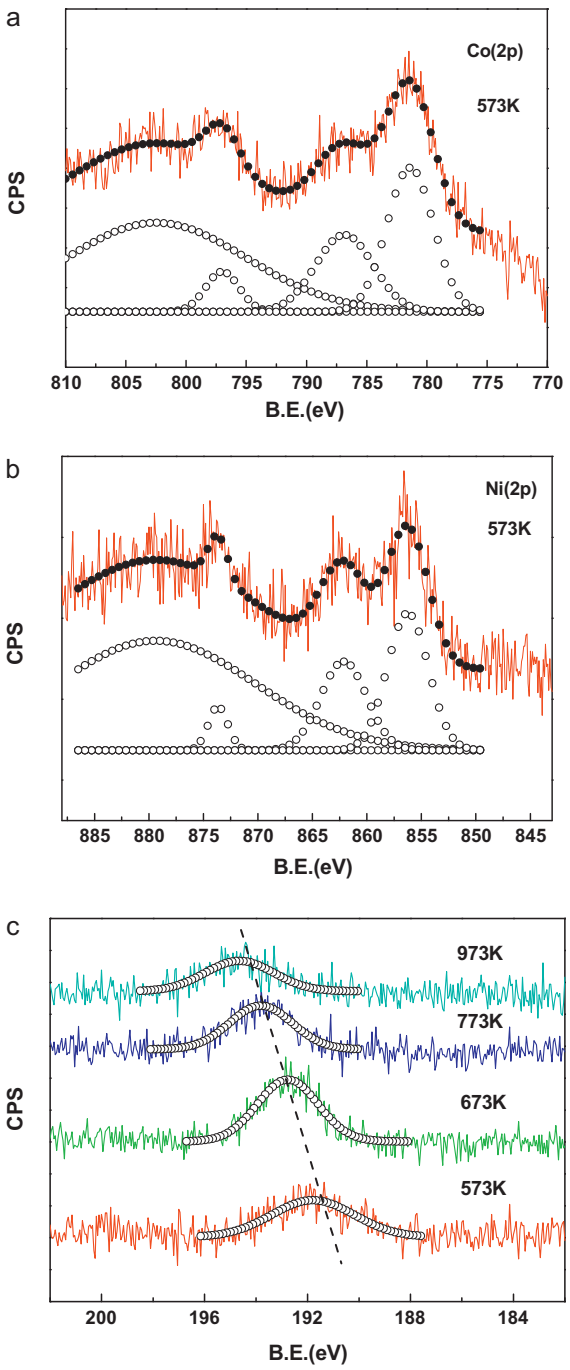

Fig. 5. Examples of the Gaussian-fitted X-ray photoelectron spectra of the Ni–Co–B catalysts: (a) Co(2p) emission for the Ni–Co–B heated at 573 K; (b) Ni(2p) emission for the Ni–Co–B heated at 573 K; and (c) B(1s) emission for all the Ni–Co–B catalysts, where the tendency of a positive shift to higher binding energy is obvious.

Ni–Co–B catalysts was carried out in a nitrogen atmosphere, which is a non-oxygen condition. Therefore, the existence of oxygen in the Ni–Co–B surface is possibly originated from washing and preserving of the as-prepared samples in air, rather than the synthesis procedure. In previous studies, Legrand et al. [33] found that Ni_2B can form oxidation product of (Ni, Ni–B, and B_2O_3) in open air; and Glavee et al. [36] found a mixture of metal $(Ni)_n$ particles and Ni_2B in nonaqueous solution under anaerobic conditions, which will converted to $(Ni)_n$ and NiO upon air exposure. The situation in this study is similar but the compositions of the catalysts are more complex. Since the catalysts here are all prepared as well as

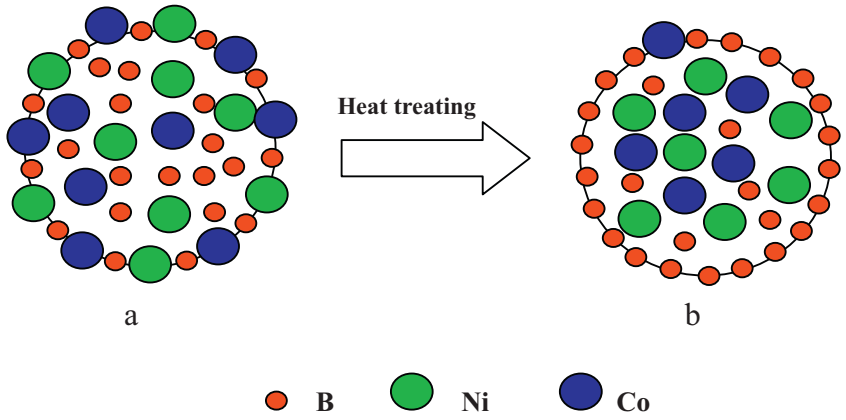

Fig. 6. Sketch map of the surface evolution of the Ni–Co–B catalyst with heat treating: (a) a normal surface with uniform metal and boron atoms at low temperatures; and (b) a boron-rich surface at high temperatures.

working in an alkaline environment, where the hydroxyl is abundant, the chemicals corresponding to peaks split from Co and Ni at the oxidation state might be CoO, Co_2O_3, $Co(OH)_2$ or NiO, Ni_2O_3, $Ni(OH)_2$, etc. This hypothesis is still need to be confirmed by further studies.

Furthermore, the Co(2p) emissions of the Ni–Co–B catalysts treated at 773 K and 973 K are very weak, as shown in Fig. 4(b); while the lack of the Ni(2p) emissions of these two Ni–Co–B catalysts are observed in Fig. 4(c). This implies the lack of metal atoms on the surface of the heavily heated Ni–Co–B catalysts. Thus, even though the samples 773 K and 973 K have abounding metal atoms in the body phase, but their surface are metal-lack and boron-rich. Therefore, the evolution of the surface structure of the Ni–Co–B catalyst has a notable change with increasing heating temperatures, as shown in Fig. 6. That is, when the heating temperature is not excess 673 K, the Ni–Co–B surface can remain a uniform distribution of the metal and boron atoms, as shown in Fig. 6(a); while the heating temperature exceeds 773 K, the Ni–Co–B surface becomes a boron-rich structure, as shown in Fig. 6(b).

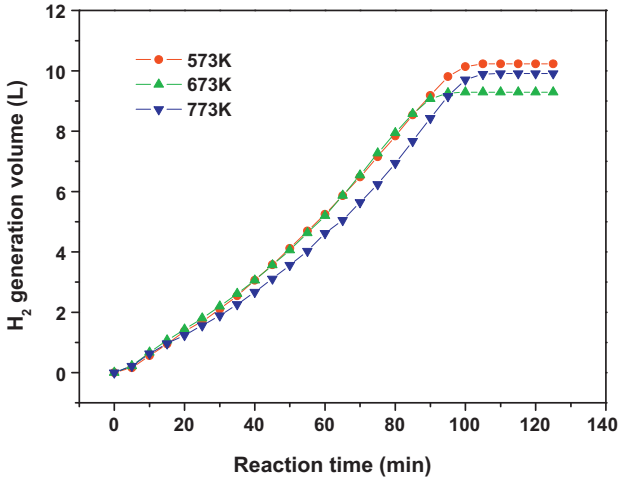

Fig. 7. Evolution of H_2 generation volume with reaction time for the Ni–Co–B heated at different temperatures.

3.5. Catalytic performance of Ni–Co–B catalysts

In Fig. 7, it can be seen that for all the Ni–Co–B catalysts treated from 573 K to 773 K, the hydrogen generation reactions have a hysteresis. This is because when the pump is switched off, some of the imported $NaBH_4$ are still not totally decomposed, and the hydrolysis reaction may last over 90 min to get the equilibrium, implying the reactions are mild and very suitable for the hydrogen supply of portable fuel cells. At last, more than 10 liters hydrogen could be released, which implies high hydrogen generation efficiencies. In addition, the hydrogen generation rates have satisfying changes. It can be seen from Fig. 8 that due to the insufficient contact between the $NaBH_4$ solution and the catalyst, the reaction rate is extremely low at the beginning, causing a part of the reaction material to accumulate in the reacting container. However, as the reaction going on, the released heat from the decomposing $NaBH_4$ causes a gradual temperature increase of the subsequent reaction, leads to the speed-up of the subsequent hydrogen generation reaction rates.

Fig. 9 shows the relationships of the average hydrogen generation rate and the heat-treating temperatures of the Ni–Co–B catalysts. It is clear that, from 373 K to 673 K, with increasing heating temperature, the hydrogen generation rate of $NaBH_4$ hydrolysis increases as well. However, it is notable in Fig. 9 that from 673 K

Table 1
Binding energies of the Ni(2p), Co(2p) and B(1s) emissions of the Ni–Co–B catalyst heat treated at various temperatures.

Heat treated temperature (K)	Binding energy (eV)						
	$Ni(2p_{3/2})$	$Ni(2p_{1/2})$	$\Delta Ni(2p)$[a]	$Co(2p_{3/2})$	$Co(2p_{1/2})$	$\Delta Co(2p)$[b]	B(1s)
573	856.2	873.7	17.5	781.3	797.1	15.8	191.8
	862.1[c]	879.4[c]	17.3	785.6	803.1	17.5	
673	856.8	874.3	17.5	782.3	798.3	17.0	192.8
	860.6[c]	881.5[c]	20.9	786.8	804.9	18.1	
773	–	–	–	–	–	–	193.8
973	–	–	–	–	–	–	194.6

[a] $\Delta Ni(2p) = Ni(2p_{1/2}) - Ni(2p_{3/2})$.
[b] $\Delta Co(2p) = Co(2p_{1/2}) - Co(2p_{3/2})$.
[c] Satellite peak.

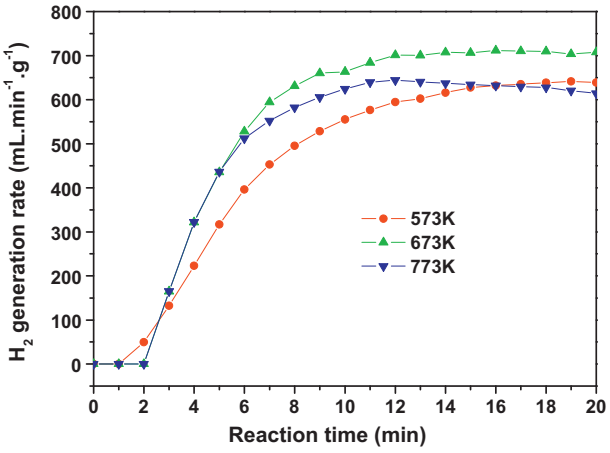

Fig. 8. Evolution of H_2 generation rate with reaction time for the Ni–Co–B heated at different temperatures.

to 973 K, when heated at high temperatures over 773 K, the average hydrogen generation rate of the Ni–Co–B catalyst decreases as well, which is indicating that the hydrogen generation rates greatly related to the heat treatment. As illustrated in Fig. 6, when the heating temperature exceeds 773 K, the Ni–Co–B surface becomes a boron-rich structure. Actually, for many metal borides, metal atoms often serve as the active centers [37], which had already been proved by our previous work [5]. Therefore, the boron-rich surface of the Ni–Co–B treated at 773 K means only few of the metal atoms exist on the surface and serve as active centers, which lead to an inferior average hydrogen generation rate. When further heated at 973 K, the Ni–Co–B with a heavy boron-rich surface has almost lost catalytic activity, as shown in Fig. 9.

For the Ni–Co–B catalyst treated at 573 K, 673 K and 773 K, the average hydrogen generation rate per unit mass could be up to 679, 708, and 615 ml min^{-1} $g^{-1}_{catalyst}$, respectively, which are all superior to crystal state Ni (19.5 ml min^{-1} $g^{-1}_{catalyst}$) and Raney Ni (228.5 ml min^{-1} $g^{-1}_{catalyst}$) [3], and thus can give successive hydrogen supply for portable PEMFCs with the power of 110, 115, and 100 W, respectively (at 100% hydrogen utilization). According to Ingersoll et al. [22], for the Ni–Co–B catalysts synthesized by a chemical reduction method, the best hydrogen generation rate by supplying fuel using peristaltic pump is only 270 ml min^{-1} $g^{-1}_{catalyst}$; while in our present work, the hydrogen generation rates of the Ni–Co–B catalyst treated from 573 K to 773 K are all superior to it. The optimized hydrogen generation performance of the Ni–Co–B catalyst treated at 673 K is originated from its uniform pore size distribution, bigger specific surface area and abundant surface active centers, as illustrated by SEM images in Fig. 2, nitrogen adsorption–desorption curves in Fig. 3, as well as the surface structure evolution sketch map in Fig. 6, which therefore result in a good contact between the catalyst and the reactant.

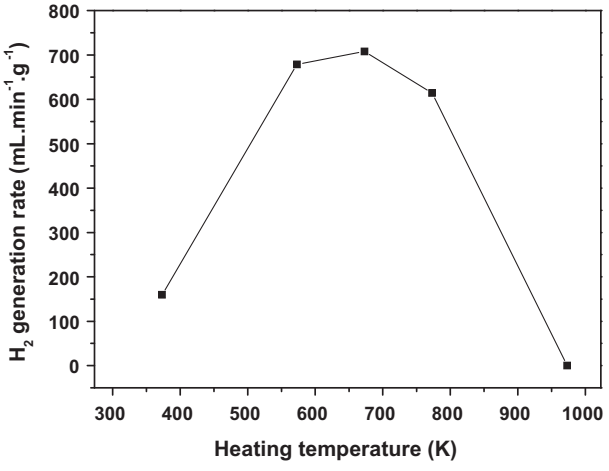

Fig. 9. Evolution of average H_2 generation rate with various heating temperatures.

4. Conclusions

A two-step technique was used for synthesizing a series of Ni–Co–B catalysts, where a chemical reduction method was used to prepare the precursors, while the heat-treatment was used to adjust the crystal structures. XRD analysis indicates the as-prepared Ni–Co–B catalysts have complex crystal structures with both amorphous and crystal compositions. Based on the XPS analysis, the shifts of the Ni($2P_{3/2}$), Co($2P_{3/2}$) and B(1s) emissions imply that the electrons of element B has transferred into the empty d orbits of Co and Ni, resulting in multiplex metal borides with highly catalytic activities, rather than simple mixture of Ni–B and Co–B. The sample heated at 673 K achieves an optimized average hydrogen generation rate of 708 ml min^{-1} $g^{-1}_{catalyst}$, which can give successive hydrogen supply for an 115 W portable PEMFC. The heavily heated catalysts over 773 K will form boron-rich and metal-lack surfaces, which are lack of active centers and not favorable to good catalytic activities.

Acknowledgements

The authors thank the National Natural Science Foundation of China (Grant no. 20806010) and the National Basic Research Program of China (Grant no. 2009CB220100) for financial support.

References

[1] C. Wu, H.M. Zhang, B.L. Yi, Catal. Today 93–95 (2004) 477–483.
[2] J. Lee, K.Y. Kong, C.R. Jung, E. Cho, S.P. Yoon, J. Han, T.-G. Lee, S.W. Nam, Catal. Today 120 (2007) 305–310.
[3] B.H. Liu, Z.P. Li, S. Suda, J. Alloys Comp. 415 (2006) 288–293.
[4] K.S. Eom, K.W. Cho, H.S. Kwon, J. Power Sources 180 (2008) 484–490.
[5] C. Wu, F. Wu, Y. Bai, B.L. Yi, H.M. Zhang, Mater. Lett. 59 (2005) 1748–1751.
[6] U.B. Demirci, F. Garin, Catal. Commun. 9 (2008) 1167–1172.
[7] N. Patel, R. Fernandes, A. Miotello, J. Catal. 271 (2010) 315–324.
[8] C. Wu, Y. Bai, F. Wu, Mater. Lett. 62 (2008) 4242–4244.
[9] C. Wu, Y. Bai, F. Wu, B.L. Yi, H.M. Zhang, Int. J. Hydrogen Energy 35 (2010) 2675–2679.
[10] Ö. Metin, S. Özkar, Int. J. Hydrogen Energy 32 (2007) 1707–1715.
[11] A. Garron, S. Bennici, A. Auroux, Appl. Catal. A: Gen. 378 (2010) 90–95.
[12] B.H. Liu, Z.P. Li, N. Morigasaki, S. Suda, Int. J. Hydrogen Energy 33 (2008) 1323–1328.
[13] S.U. Jeong, R.K. Kim, E.A. Cho, H.-J. Kim, S.-W. Nam, I.-H. Oh, S.-A. Hong, S.H. Kim, J. Power Sources 144 (2005) 129–134.
[14] Y.Q. Huang, Y. Wang, R.X. Zhao, P.K. Shen, Z.D. Wei, Int. J. Hydrogen Energy 33 (2008) 7110–7115.
[15] B.H. Liu, Q. Li, Int. J. Hydrogen Energy 33 (2008) 7385–7391.
[16] H.J. Tian, Q.J. Guo, D.Y. Xu, J. Power Sources 195 (2010) 2136–2142.
[17] H. Ma, W.Q. Ji, J.Z. Zhao, J. Liang, J. Chen, J. Alloys Comp. 474 (2009) 584–589.
[18] P. Krishnan, S.G. Advani, A.K. Prasad, Appl. Catal. B: Environ. 86 (2009) 137–144.
[19] S.U. Jeong, E.A. Cho, S.W. Nam, I.H. Oh, U.H. Jung, S.H. Kim, Int. J. Hydrogen Energy 32 (2007) 1749–1754.
[20] H. Dong, H.X. Yang, X.P. Ai, C.S. Cha, Int. J. Hydrogen Energy 28 (2003) 1095–1100.
[21] C. Wu, Y. Bai, F. Wu, G.Q. Wang, Trans. Nonferric Met. Soc. China 17 (2007) s1002–s1005.
[22] J.C. Ingersoll, N. Mani, J.C. Thenmozhiyal, A. Muthaiah, J. Power Sources 173 (2007) 450–457.
[23] R. Fernandes, N. Patel, A. Miotello, M. Filippi, J. Mol. Catal. A: Chem. 298 (2009) 1–6.
[24] J.F. Geng, D.A. Jefferson, B.F.G. Johnson, Chem. Eur. J. 15 (2009) 1134–1143.
[25] JCPDS 87-0712.
[26] JCPDS 15-806.
[27] JCPDS 65-2410.
[28] JCPDS 39-1107.
[29] JCPDS 17-0335.
[30] C. Wu, Y. Bai, X. Wang, F. Wu, C.Z. Zhang, Solid State Ionics (179) (2008) 924–927.

[31] H.X. Li, Y.D. Wu, H.S. Luo, M.H. Wang, Y.P. Xu, J. Catal. 214 (2003) 15–25.
[32] W.L. Dai, M.H. Qiao, J.F. Deng, Appl. Surf. Sci. 120 (1997) 119–124.
[33] J. Legrand, A. Taleb, S. Gota, M.-J. Guittet, C. Petit, Langmuir 18 (2002) 4131–4137.
[34] A. Levy, J.B. Brown, C.J. Lyons, Ind. Eng. Chem. 52 (1960) 211–214.
[35] C. Wu, Y. Bai, F. Wu, L.W. Dong, X. Wang, L.X. Yang, C.Z. Zhang, Electrochim. Acta 53 (2008) 4715–4720.
[36] G.N. Glavee, K.J. Klabunde, C.M. Sorensen, G.C. Hadjipanayis, Langmuir 10 (1994) 4726–4730.
[37] J.J. Burton, R.L. Garten, Advanced Materials in Catalysis, 2nd ed, London Academic Press, 1977.